Polymers

Effect of amorphous carbon on the tensile behavior of polyacrylonitrile (PAN)-based carbon fibers

Fenghao Yang[1] , Guangmin Hu[1] , Haoyuan He[1] , Maozhong Yi[1,*] , Yicheng Ge[1] , Liping Ran[1] , and Ke Peng[1]

[1] State Key Laboratory of Powder Metallurgy, Central South University, Changsha 410083, People's Republic of China

ABSTRACT

The effects of the microstructure evolution of amorphous carbon on the tensile behavior of polyacrylonitrile (PAN)-based carbon fibers were investigated. The microstructure as a function of heat treatment temperature was characterized by means of XRD, HRTEM and Raman spectra. It is found that the amorphous carbon content decreases with increasing heat treatment temperature and that the densities of the carbon fibers increase is due to the removal of the impurity elements and the shrinking of the graphite planes. The amorphous carbon parallel to the graphite planes transforms into graphite planes and stacks on the graphite crystallites, leading to the increase in the graphite crystallite thickness. And the graphite crystallite length is increased through the amorphous-to-crystallite transition which occurs at the edges of graphite planes and the coalescence between two adjacent graphite crystallites. It is found that the tensile behavior of PAN-based carbon fibers mainly depends on the microstructure evolution of amorphous carbon. The reactions between sp^2 carbon clusters and graphite planes improve the cross-linking among graphite crystallites, which has a positive effect on the tensile strength of the carbon fibers. However, a large number of structural defects and residual stresses, introduced by the rearrangement of graphite planes, are the main reasons for the degradation of the tensile strength. The tensile strains of the carbon fibers decrease and the tensile modulus increase with the decrease in the amorphous carbon content, which are mainly due to the amorphous-to-crystallite transition in the skin region.

Introduction

Polyacrylonitrile (PAN)-based carbon fibers are widely used as reinforcements in carbon/carbon composites, owing to their ultrahigh strength and stiffness, light weight and high-temperature performance [1–8]. Since carbon fibers act as main constitutive units, the mechanical properties of carbon/carbon composites strongly depend on the properties of the carbon fibers and the fiber/matrix bonding strength [9–11]. During the fabrication of carbon/carbon composites, the carbon fibers undergo

Address correspondence to E-mail: yimaozhong@126.com

complex thermal processes such as chemical vapor infiltration, impregnation/carbonization and graphitization [12, 13]. It is well known that the skin–core heterogeneity of PAN-based carbon fibers depends on the thermal processes during manufacturing, i.e., the structural integrity of graphite crystallites and the orientation of graphite planes gradually decrease from the skin region to the core region [14–17]. Many studies have also shown that an increase in the skin–core heterogeneity of carbon fibers would degrade the fiber strength after high-temperature heat treatment [18, 19]. However, there is very little information available in the literature concerning the effects of the thermal processes on the properties of carbon fibers. Therefore, the microstructure and mechanical properties of carbon fibers heat-treated at carbonization and graphitization temperatures are required for the design and performance prediction of carbon/carbon composites.

In order to obtain high-performance PAN-based carbon fibers, extensive researches have been carried out on their structure–property relationship during carbonization and graphitization [20–24]. The tensile strength of carbon fibers usually decreases with the increase in their tensile modulus, which is mainly ascribed to the increase in size and orientation of the graphite crystallites with increasing heat treatment temperature [22, 25, 26]. Moreover, the surface defects, structure defects and microvoids of carbon fibers generated during their manufacture processes may also greatly degrade their tensile strength and tensile modulus [17]. In fact, except for a small amount of microvoids, the volume fraction of the graphite crystallites in carbon fibers is about 0.4–0.8, indicating that a lot of amorphous carbon (disordered regions) exists [27]. Since the amorphous carbon as a matrix plays an important role in transferring load during tensile, its effect on the mechanical properties of carbon fibers cannot be ignored. Recently, the fact that a nanocomposite mechanical model only took into account the properties of both the graphite crystallites and the amorphous carbon has successfully explained the dependence of the tensile strength, tensile modulus and compressive strength of PAN-based carbon fibers on their microstructure [1, 27–30]. It is suggested that the microstructure of the amorphous carbon is a key factor in further improving the performances of carbon fibers. Thus, it is necessary to investigate both the microstructure evolution of the amorphous carbon in the skin and in the core regions of PAN-based carbon fibers during heat treatment and its effect on the tensile behavior.

In this paper, PAN-based carbon fibers were heat-treated at carbonization and graphitization temperatures and the microstructure evolution of amorphous carbon in the skin and in the core regions was studied. Raman spectroscopy based on lattice vibrations is a prominent tool to identify these disordered structures, which can provide quantitative information about the amorphous carbon [31–34]. Finally, the Raman spectra of the carbon fiber surfaces were recorded and the spectral parameters related to their disordered structural information were discussed. Furthermore, the effect of the microstructure evolution of amorphous carbon on the tensile behavior of the carbon fibers was investigated.

Experimental

Preparation of the materials

Commercially available 3 K PAN-based T300 carbon fibers (Weihai Tuozhan Fiber Co., Ltd. Weihai, China) were used in this study. Before the specimen preparation, the sizing agent on the fiber surface was removed using the Soxhlet extraction method and the carbon fibers were immersed in a mixed solution of acetone and ethanol with the volume ration of 1:1 for 2 days at 80 °C. The typical properties of the as-received carbon fibers were examined by a single-fiber test, and the results are shown in Table 1. The density and diameter of the as-received carbon fibers were 1.76 g/cm^3 and 7.0 μm, respectively. The cross section of the as-received fibers exhibited a bean shape (see Fig. 1).

Given that the carbon fiber fabrics should be heat-treated at carbonization temperatures before preparing the carbon/carbon composites, an appropriate heat treatment temperature is critical to remove impurity elements and avoid the degradation of carbon fiber properties. Therefore, the carbon fibers were heat-treated at three different carbonization temperatures of 1200 °C, 1400 °C and 1600 °C. The graphitization temperatures were 1800 °C, 2100 °C and 2300 °C. The as-received and heat-treated PAN-based carbon fibers were named as CF1–CF7 in turn (see Table 2). The specimens were heated in a graphitization furnace (Advanced Corporation for Materials & Equipments Co., Ltd. Changsha, China)

Table 1 Typical properties of the as-received carbon fibers

	Tensile strength, σ (GPa)	Tensile modulus, E (GPa)	Tensile strain, ε (%)	Density (g/cm^3)	Diameter (μm)
As-received carbon fibers	3.05 ± 0.63	180 ± 20	1.74 ± 0.24	1.76	7.0

Figure 1 Morphologies of the **a** surface and **b** cross section of the as-received carbon fibers.
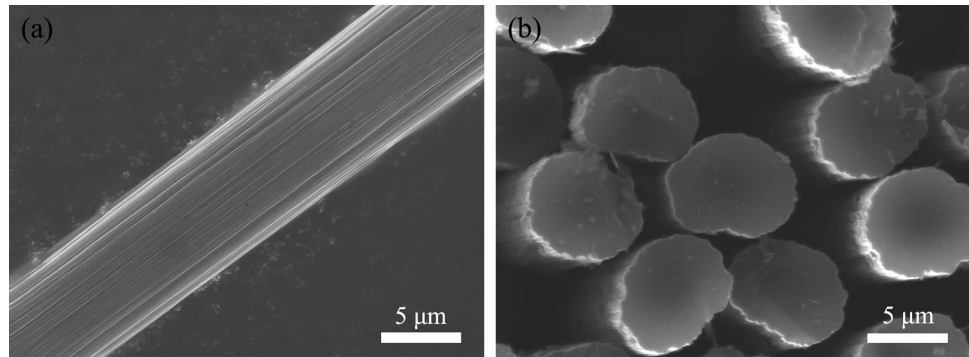
Table 2 Amorphous carbon content, impurity element contents (nitrogen, oxygen and hydrogen), and densities of the as-received and heat-treated PAN-based carbon fibers

Specimens	Heat treatment temperature (°C)	Amorphous carbon content (wt%)	Nitrogen content (wt%)	Oxygen content (wt%)	Hydrogen content (wt%)	Density (g/cm^3)
CF1	As-received	35.9	6.29	0.56	0.25	1.76
CF2	1200	35.4	3.32	0.37	0.03	1.77
CF3	1400	28.6	1.20	0.23	0.01	1.79
CF4	1600	27.1	0.31	0.20	0.01	1.79
CF5	1800	20.5	0.08	0.17	##	1.80
CF6	2100	11.6	0.07	0.16	##	1.86
CF7	2300	9.9	0.08	0.17	##	1.88

with a hot zone of Φ 200 × 500 mm. The specimens were held at the desired temperature for 2 h with a heating rate of 10 °C/min and then cooled in the furnace. During the heat treatment, the vacuum was controlled at 10^{-1} Pa.

Characterization

The graphite crystallite structure of carbon fibers was analyzed by a Bruker D8 ADVANCE X-ray diffraction (XRD, Cu Kα, $\lambda = 0.154$ nm). The acceleration voltage and emission current were 40 kV and 40 mA, respectively. The range of the 2θ values was from 10° to 60° and the scan speed was 3 °/min. The air scattering was subtracted from the diffraction profile

of the specimens. The diffraction curve was fitted with a Voigt function to get peak position and full width at half maximum (FWHM). The graphite crystallite parameters L_c and L_a were calculated using Debye–Scherrer equation from the positions and FWHM of the (002), (100) peaks, respectively [20]. The values of the interlayer spacing $d_{(002)}$ were measured by Bragg's law. Because the microstructure of the carbon fibers consists of the graphite crystallites and amorphous phase, the diffraction intensity of the (002) peak can be regarded as the sum of the diffraction intensities of the crystallite phase and the amorphous phase (see Fig. 2). Because the diffraction peak of the amorphous phase and the crystallite phase was closely overlapped, the separation of the
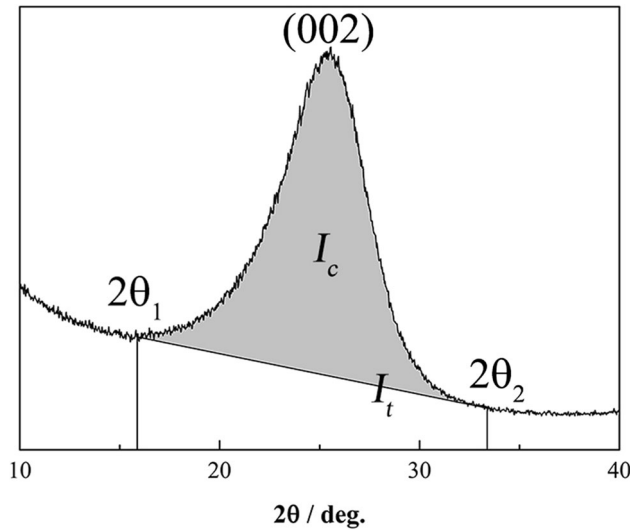
Figure 2 Diffraction intensity of the (002) peak.

diffraction peaks may result in large statistical uncertainty. Therefore, the amorphous carbon content was defined as [35]:

$$f = \frac{I_t - I_c}{I_t} \times 100\% \tag{1}$$

where I_c was the integral intensity of the (002) peak and I_t was the integral intensity of the total scattering.

The tensile behavior of carbon fibers was investigated using a single-fiber tensile test according to ISO11566-1996. The single fiber was fixed on a rectangular paper holder and the gauge length was 25 mm. Then, the sample was placed on the grips of an electronic single-fiber strength tester (YG-001A, Taicang Hongda Textile Instrument Co., Ltd. Taicang, China) with a load cell of 100 cN. The edges of the paper holder were cut, and a crosshead speed of 0.5 mm/min was applied. Tensile tests were carried out on at least 50 single fibers for each specimen. Each fiber diameter was measured using a Leica optical microscopy. The tensile strain was calculated from the ratio of the tensile elongation to the original length, and the tensile elongation was corrected by a system compliance [36]. For each specimen, the tensile strength (σ_i) and tensile modulus (E) were calculated by:

$$\sigma_i = \frac{F_i}{A_i} \tag{2}$$

$$E = \frac{\Delta\sigma}{\Delta\varepsilon} \tag{3}$$

where F_i was the maximum tensile force and A_i was the cross-sectional area. The tensile fracture surfaces were observed using a scanning electron microscope (SEM, FEI Helios Nanolab 600i). The tensile strength distribution of the carbon fibers can be analyzed by the well-known Weibull model [1, 29]:

$$F = 1 - \exp[-(\sigma/\sigma_0)^m] \tag{4}$$

where F was the failure probability, σ was the fracture stress, σ_0 was the scale parameter, and m was the Weibull modulus parameter. By taking the natural logarithms, the rearrangement of Eq. (4) gave the following equation:

$$\ln\left[\ln\frac{1}{1-F}\right] = m\ln\sigma - m\ln\sigma_0 \tag{5}$$

If we use a straight line to fit the Weibull expression, the Weibull modulus and scale parameters can be calculated by the slope and y-intercept of the line. The tensile strength (σ) and standard deviation (S) can be calculated by the following equation:

$$\sigma = \sigma_0\Gamma(1 + 1/m) \tag{6}$$

$$S = \sigma_0\sqrt{\Gamma\left(1 + \frac{2}{m}\right) - \Gamma^2\left(1 + \frac{1}{m}\right)} \tag{7}$$

where Γ was the Gamma function.

Elemental analysis (LECO TCH-600) was performed to measure the amount of impurity elements such as nitrogen, hydrogen and oxygen in carbon fibers. The carbon fibers were ultrasonically cleaned with deionized water and then were dried in a vacuum oven at 80 °C before Elemental analysis. Each specimen was measured no less than twice to ensure that the statistical deviation did not exceed 1%. Densities of the carbon fibers were measured by the flotation technique. Dibromoethane (2.18 g/cm³) and carbon tetrachloride (1.60 g/cm³) were mixed in a certain proportion to ensure that the carbon fibers were suspended in the mixture for at least 4 h at 25 °C. The density of the mixture, which was equal to the specimen density, was obtained by a pycnometer method. Longitudinal sectional slices of carbon fibers were obtained by focused ion beam machining (FIB, FEI Helios Nanolab 600i) and observed using a high-resolution transmission electron microscopy (HRTEM, Titan G2 60-300).

The Raman spectra of the carbon fiber surfaces were performed under a Raman microscope system (LabRAM ARAMIS) equipped with an Ar ion laser (wavelength $\lambda = 532$ nm). The diameter of the laser spot on the fiber surface was 1 μm, and the analyzed

region was magnified by a 50×/0.50 objective. In order to avoid the laser heating effect, the laser power on the fiber surfaces was kept no more than 5 mW. The Raman spectra were recorded from 1000 to 1800 cm^{-1} with a spectral resolution of 1 cm^{-1}. Acquisition time was 20 s, and three spectra were recorded for each specimen. The Raman spectra were analyzed using a Voigt function to obtain accurate spectral parameters.

Results and discussion

Microstructure evolution

Figure 3 shows the XRD patterns, interlayer spacing $d_{(002)}$ and graphite crystallite parameters of the as-received and heat-treated PAN-based carbon fibers. It is noted that the interlayer spacing $d_{(002)}$ generally decreases, indicating that the graphite crystallites change from a turbstratic structure to an ordered alignment and the graphite planes would shrink. The graphite crystallite parameters L_c and L_a, which represent the average thickness and the average length of the graphite crystallites, respectively, increase with increasing the heat treatment temperature (see Fig. 3c), while the amorphous carbon content decreases. Compared to the carbonization heat treatment, the amorphous carbon content was reduced to 9.9 wt% after heat treatment at 2300 °C (see Table 2). Because the graphite crystallite is the most thermodynamically stable phase in carbon fibers, some amorphous carbon has transformed into graphite crystallites during heat treatment.

The impurity element contents (nitrogen, oxygen and hydrogen) and densities of the as-received and
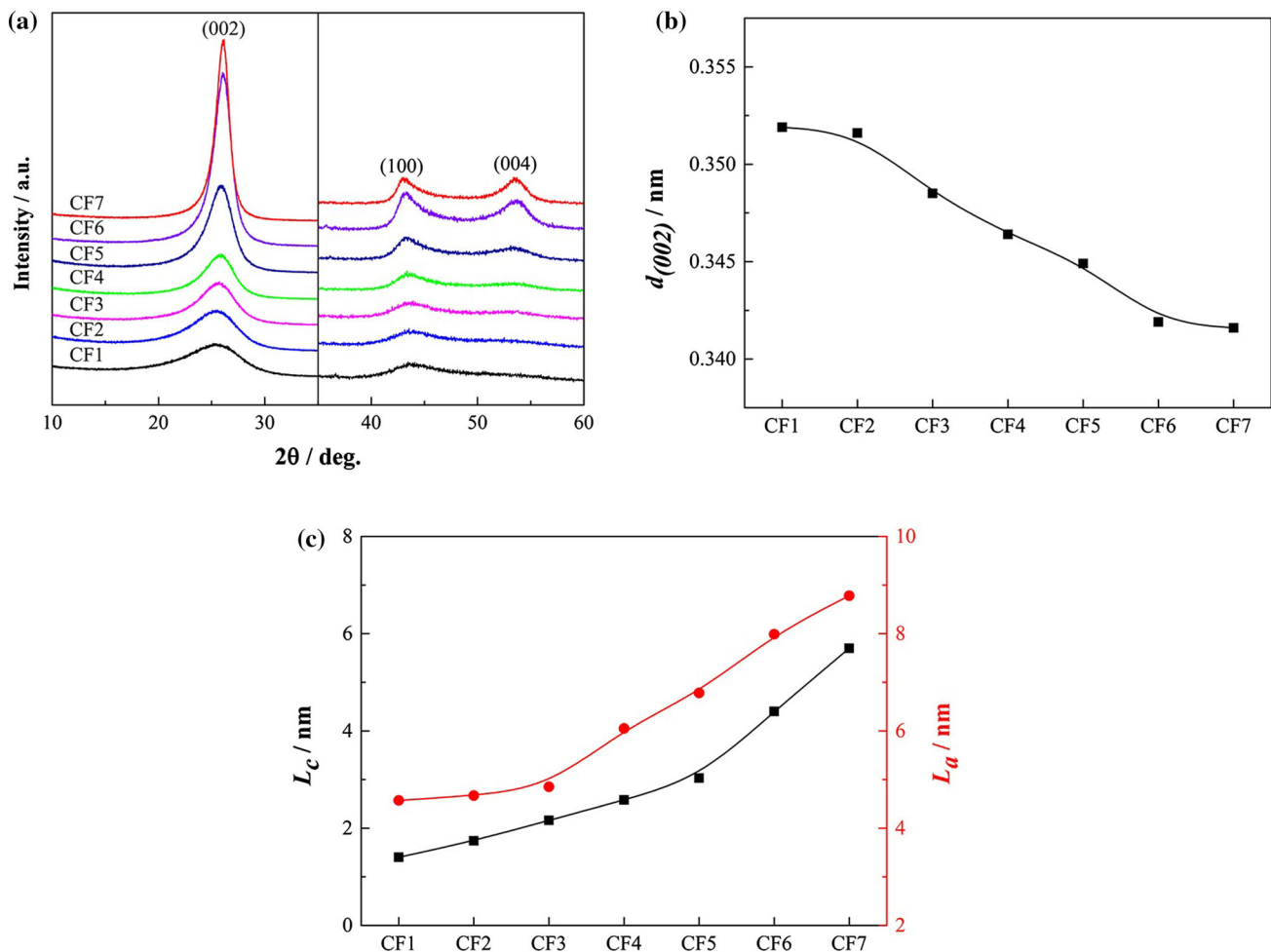

Figure 3 a XRD patterns, b interlayer spacing $d_{(002)}$ and c graphite crystallite parameters of the as-received and heat-treated PAN-based carbon fibers, respectively.

heat-treated PAN-based carbon fibers are shown in Table 2. It can be seen that a large amount of nitrogen, oxygen and all hydrogen element have been removed during carbonization heat treatment. When the carbon fibers were heat-treated at graphitization temperatures, there is almost no change in nitrogen and oxygen contents. Among these impurity elements, the nitrogen element has a big effect on the cross-linking among graphite crystallites [37]. The nitrogen atoms in carbon fibers may exist in three forms: (a) substituted carbon atoms in the aromatic rings; (b) located in the aromatic rings bonded together across the graphite planes; (c) located at the edges of the graphite planes [37–39]. The last type of nitrogen atoms is easily removed, which can form a lot of active dangling bonds at the edges of the graphite planes. These dangling bonds would react with short-range sp^2 carbon or sp^3 carbon to form graphite planes, which is an important reason for the increase in the graphite crystallites. The densities of the carbon fibers increase from 1.76 to 1.88 g/cm^3 with increasing heat treatment temperature, which is attributed to the removal of the impurity elements and the shrinking of the graphite planes.

Figure 4 shows the HRTEM images of the graphite crystallites and amorphous carbon in the skin and in the core regions. In the HRTEM images, some lattice fringes with regular arrangement represent graphite crystallites, which are marked by dotted rectangles. Some disordered structures, known as amorphous carbon, are marked by dotted ellipses. Because the basic structural unit of carbon fibers is turbostratic graphite planes, there are no clear boundaries between the graphite crystallites and the amorphous carbon in specimen CF1. The typical graphite plane length is short both in the skin and in the core regions, and their alignments are irregular and curve along the fiber axis. Though the morphology of the amorphous carbon is ambiguous, a small amount of short-range sp^2 carbons could be found in these disordered regions. Okuda et al. [34] suggested that PAN-based carbon fibers mainly consist of sp^2 carbon layers (graphite crystallite) and sp^2 carbon clusters (carbon-like component). Therefore, it could be inferred that the microstructure of the amorphous carbon consists of sp^2 carbon clusters and sp^2-bonded amorphous carbon.

Compared with specimen CF1, the boundaries between the graphite crystallites and the amorphous carbon become clearer in specimen CF4 (Fig. 4c, d).

The amorphous carbon primarily distributes in two regions: one is parallel to the stacking graphite planes (AC1) and the other is where graphite planes are interconnected or cross-linked (AC2). That a lot of ordered graphite planes parallel to the fiber axis appear is due to the amorphous-to-crystallite transition, indicating that the turbostratic graphite structure gradually transforms into a three-dimensional graphite structure. In the core region, because the arrangement of the graphite planes is relatively curved or twisted, the AC1 and AC2 are randomly distributed around the graphite crystallites (see Fig. 4d). When the carbon fibers were heat-treated at graphitization temperature, the rearrangement of the graphite planes is accelerated due to the high thermal activation, leading to a quasi perfect graphite plane stacking (see Fig. 4e, f). In comparison with graphite planes in the skin region, the stacking order of the graphite planes is wrinkled along the fiber axis in the core region. Given that the graphite crystallites with similar orientation would coalesce into an extended network, the continuity of the graphite crystallites is improved. If the orientation of adjacent graphite crystallites is quite different, the AC2 would develop into structural defects such as grain boundaries, dislocation and stacking fault.

Clearly, the increases in the graphite crystallite thickness and length have a close relationship with the distribution and microstructure evolution of amorphous carbon. The sp^2 carbon clusters in AC1 form large graphite planes and stack parallel to the graphite planes, resulting in the increase in the graphite crystallite thickness. The increase in the graphite crystallite length is attributed to the transformation of AC2 and the coalescence between two adjacent graphite crystallites. Basal planes are formed by long-range ordered graphite planes which are generated by the bridge of several graphite planes. Because the graphite planes should be stacked parallel to the basal planes, the orientation of the graphite crystallites is improved both in the skin and in the core regions.

Raman spectra analysis

The microstructure transformation of amorphous carbon into graphite crystallites can be speculated based on the HRTEM results; however, it was difficult to provide quantitative information on the different forms of amorphous carbon existed in the

Figure 4 HRTEM images of the graphite crystallites and amorphous carbon in the skin and in the core regions: **a**, **b** CF1, **c**, **d** CF4, **e**, **f** CF7.
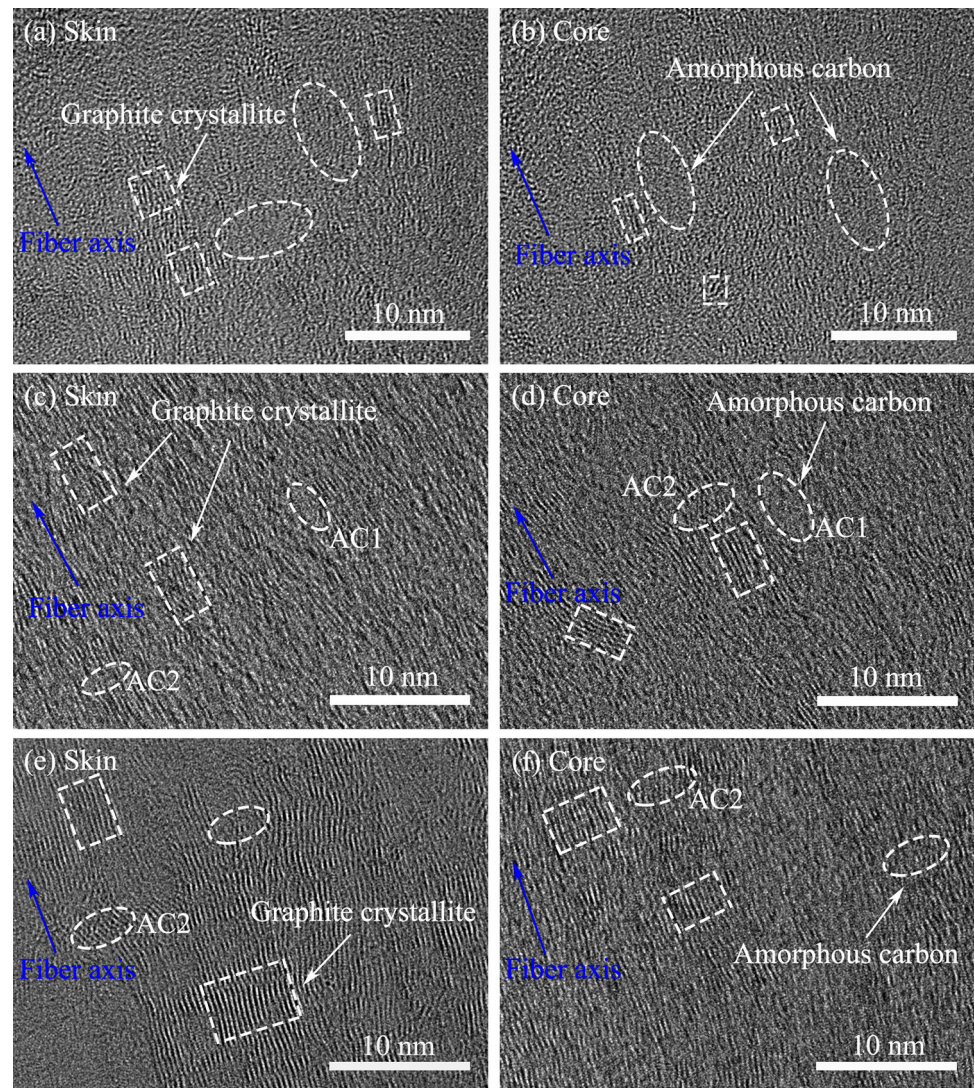
carbon fibers. The first-order Raman spectra of the carbon fiber surfaces between 1000 and 1800 cm^{-1} are illustrated in Fig. 4. The spectra of the carbon fiber surfaces exhibit two overlapping peaks that are separated from each other with the decrease in the amorphous carbon content. In order to quantitatively analyze and determine the spectral parameters such as band position, band width and band intensity, curve fitting results of the Raman spectra with a Voigt line shape are given in Fig. 5. The fitting considered five first-order Raman bands of carbon materials (D1–D4 and G bands, see Table 3). Since the detection depth of Raman spectroscopy is about 100 nm [3], the structural information extracted from the Raman spectra is closely related to the microstructure in the skin region of the carbon fibers.

The G ("Graphite") band at around 1580 cm^{-1} is an ideal graphitic lattice vibration and corresponds to the stretching vibration in the aromatic layers. The peak appeared at around 1360 cm^{-1} is known as the D1 ("Disorder-induced") band, which originates from a disordered graphitic lattice vibration at the edge of a graphite plane. Because the length and the ordering of the graphite planes gradually increase, the FWHMs of the D1 and G bands decrease (see Fig. 6a). The D4 band, as a low-frequency shoulder of the D1 band, is assigned to the presence of sp^2–sp^3 bands or C–C and C=C stretching vibrations of polyene-like structures [33], which cannot be detected in the specimen CF6 and CF7, indicating that those disordered structures completely disappear in the skin region. Another band between the D1 and G bands is the D3 band at 1525 cm^{-1}, which derives from sp^2-
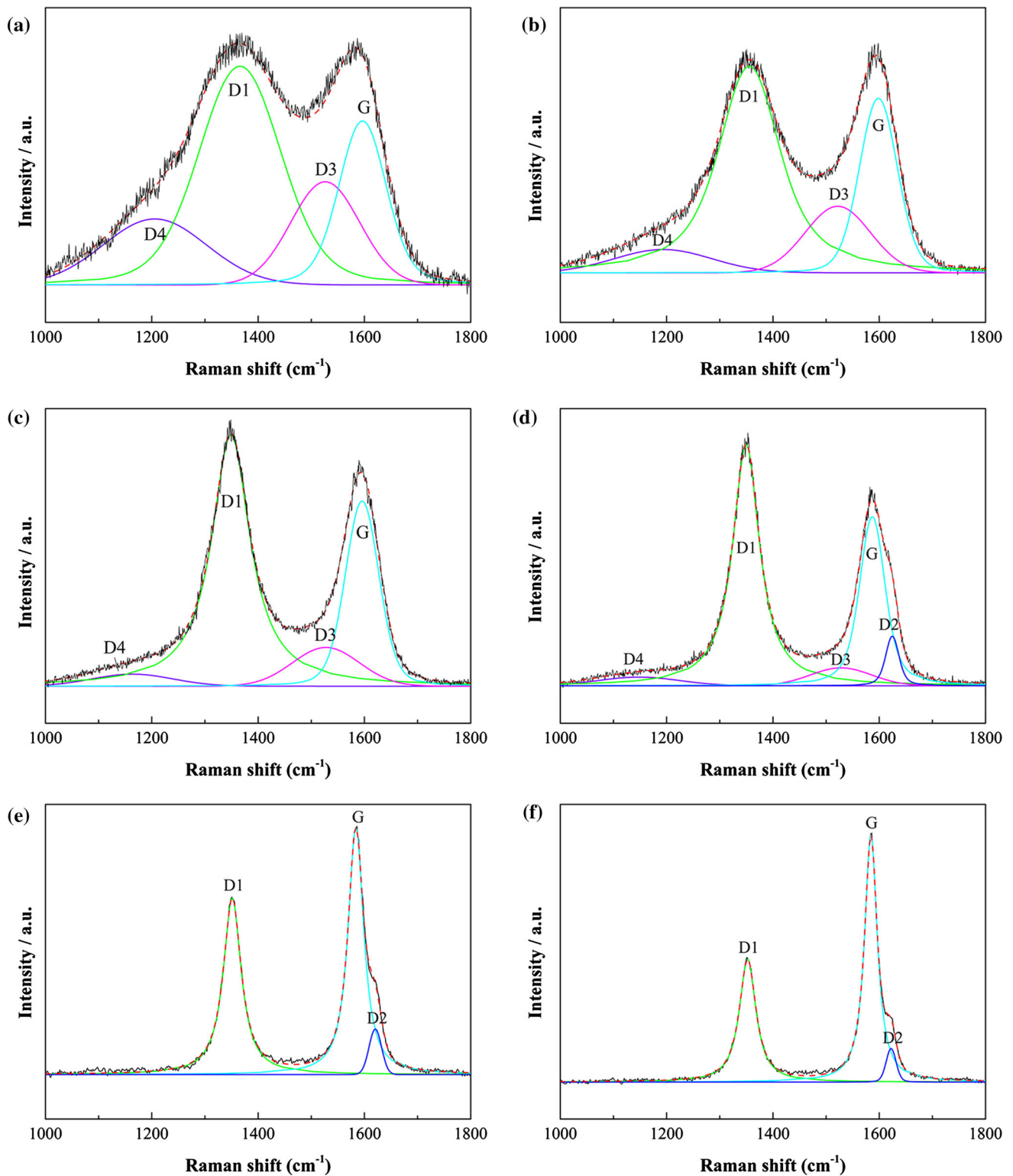
Figure 5 Curve fitting results of the Raman spectra: **a** CF1, **b** CF3, **c** CF4, **d** CF5, **e** CF6 and **f** CF7.

bonded amorphous carbon [31]. Obviously, for the graphitized carbon fibers, that the D3 bands fail to be separated from the overlapping D1 and G bands is

due to the large reduction in amorphous carbon content. There is no significant difference among the FWHMs of the D3 bands, which is primarily due to

Table 3 First-order Raman bands and vibration modes of carbon materials [31–33]

Band	Raman shift (cm^{-1})	Vibration mode
D4	~ 1200	Disordered graphitic lattice (A1g symmetry)
D1	~ 1350	Disordered graphitic lattice (A1g symmetry)
D3	~ 1500	Amorphous carbon
G	~ 1580	Ideal graphitic lattice (E2g symmetry)
D2	~ 1620	Disordered graphitic lattice (E2g symmetry)
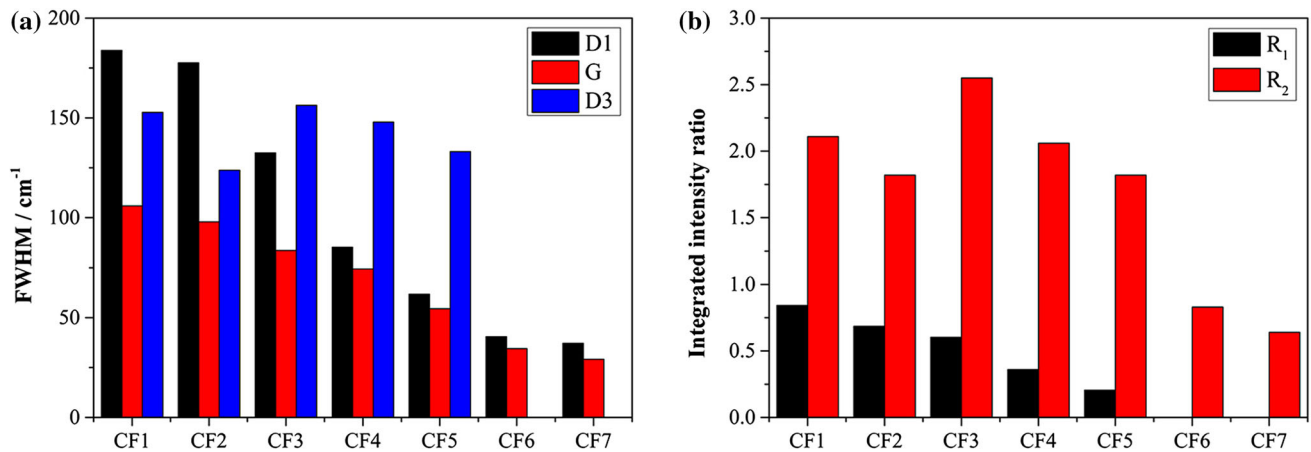
Figure 6 **a** FWHM of the D1, D3 and G bands; **b** integrated intensity ratios: $R_1 = I_{D3}/I_G$ and $R_2 = I_{D1}/I_G$.

the high statistical uncertainty of the separation of the D1 and G bands. The analysis of Raman intensities is meaningful since it can provide more structural information about amorphous carbon.

Here, the integrated intensity ratio $R_1 = I_{D3}/I_G$ was adopted as a structural disorder parameter to explain the structural information of the carbon fibers. The disorder parameter R_1 represents the relationship between sp^2-bonded amorphous carbon and graphite crystallites. In Fig. 6b, it is apparent that the disorder parameter R_1 decreases, which suggests that the sp^2-bonded amorphous carbon has transformed into ordered graphite crystallites during heat treatment. This result is consistent with the amorphous-to-crystallite transition in the skin region. Several earlier studies have reported that the degree of graphitization is related to the band intensity ratio $R_2 = I_{D1}/I_G$ [31, 32, 34]. The integrated intensity ratio R_2 of specimen CF3 has a maximum value of about 2.54, indicating that its disordered graphitic lattice vibration is high. It could be inferred that the point defect due to the removal of nitrogen would destroy the integrity of graphite crystallites and increase the activity of the D1 band. Obviously, the elimination of the point defect and the improvement in the ordering of the graphite planes are the main reasons to explain

why the R_2 decreases to 0.64 at graphitization temperature (see Fig. 6b).

Tensile property

Figure 7 shows the tensile fracture surfaces of the carbon fibers. As can be seen, the tensile fracture surfaces of the carbon fibers show a typical Griffiths brittle fracture. The features of the tensile fracture surfaces are similar, including a fracture source and fracture grooves formed by the crack propagation. The fracture sources of these carbon fibers are primarily located on the fiber surface or near-surface region, which indicates that the distribution of defects and the microstructure in the skin region are important factors in controlling the tensile behavior of the carbon fibers. Taking into account the crack propagation path, the fracture surfaces show a radial fracture region and an irregular fracture region. When the carbon fibers contain a lot of amorphous carbon, cracks may propagate along the axial and radial directions of the carbon fibers, and thus the fracture surfaces of specimen CF1 and CF4 are of great roughness. However, for the graphitized carbon fibers, it is clear that the fracture surface is granular and the radial fracture grooves almost cover the

Figure 7 Tensile fracture surfaces of the carbon fibers: **a** CF1, **b** CF4, **c** CF6, **d** CF7.
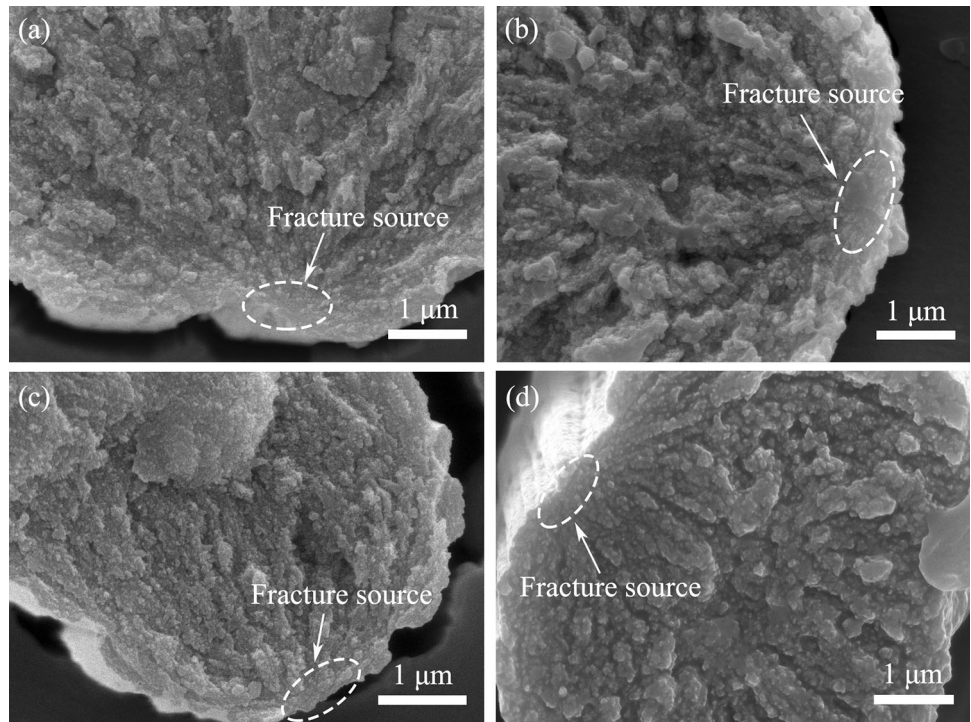
whole fracture surface (see Fig. 7d). The granular structure is considered to be a dense alignment of the graphite crystallites. The cracks prefer to propagate along the structural defects of graphite crystallites and the edges of the granular structure.

The Weibull plots of the as-received and heat-treated PAN-based carbon fibers are presented in Fig. 8, and the corresponding Weibull parameters are presented in Table 4. The Weibull modulus can be regarded as a distribution of the defects that controls
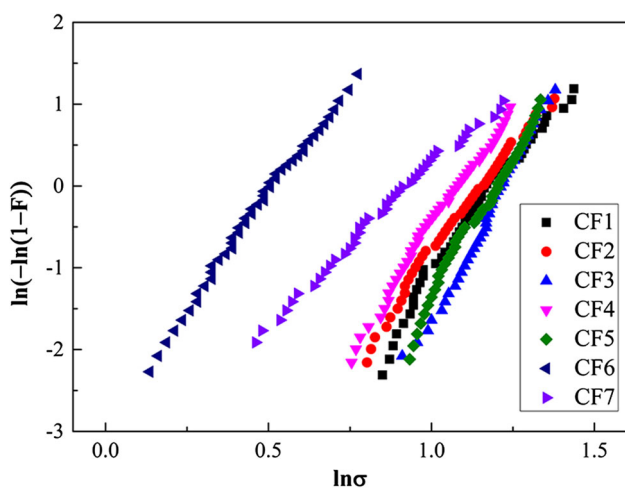

**Figure 8** Weibull plots of the as-received and heat-treated PAN-based carbon fibers.

the tensile strength of carbon fibers [36]. The specimen CF3 has a maximum tensile strength and Weibull modulus, which could be inferred that it has the least defects that are evenly distributed in the carbon fibers. Moreover, when the sp^2 carbon clusters are bonded to the edges of graphite planes, the cross-linking among graphite crystallites would be enhanced, which is beneficial to improving the tensile strength of the carbon fibers. However, after graphitization, the tensile strength decreases intensely to 1.55 GPa, which is believed to be caused by the structural defects that occur during the rearrangement of the graphite planes. The decrease in the Weibull modulus has also confirmed the result. Moreover, the residual stresses, which might be generated by the large difference in the thermal expansion coefficients perpendicular or parallel to the graphite plane, could also cause the strength degradation of the carbon fibers. The tensile strength of specimen CF7 is improved, which is primarily attributed to the increase in the continuity of the graphite crystallites.

Effect of the amorphous carbon on the tensile behavior

Table 4 shows the tensile strains and the tensile modulus of the as-received and heat-treated PAN-

Table 4 Weibull parameters and tensile properties of the as-received and heat-treated PAN-based carbon fibers

Specimens	Weibull modulus, m	Scale parameter, σ_0 (GPa)	Tensile strength, σ (GPa)	Tensile modulus, E (GPa)	Tensile strain, ε (%)
CF1	5.58	3.30	3.05 ± 0.63	180 ± 20	1.74 ± 0.24
CF2	5.38	3.18	2.93 ± 0.63	189 ± 19	1.62 ± 0.26
CF3	7.71	3.38	3.18 ± 0.49	213 ± 24	1.53 ± 0.20
CF4	6.00	2.96	2.74 ± 0.53	225 ± 28	1.25 ± 0.20
CF5	6.90	3.13	3.10 ± 0.53	246 ± 25	1.30 ± 0.17
CF6	5.56	1.68	1.55 ± 0.32	218 ± 31	0.87 ± 0.22
CF7	3.91	2.55	2.30 ± 0.66	252 ± 28	1.03 ± 0.19
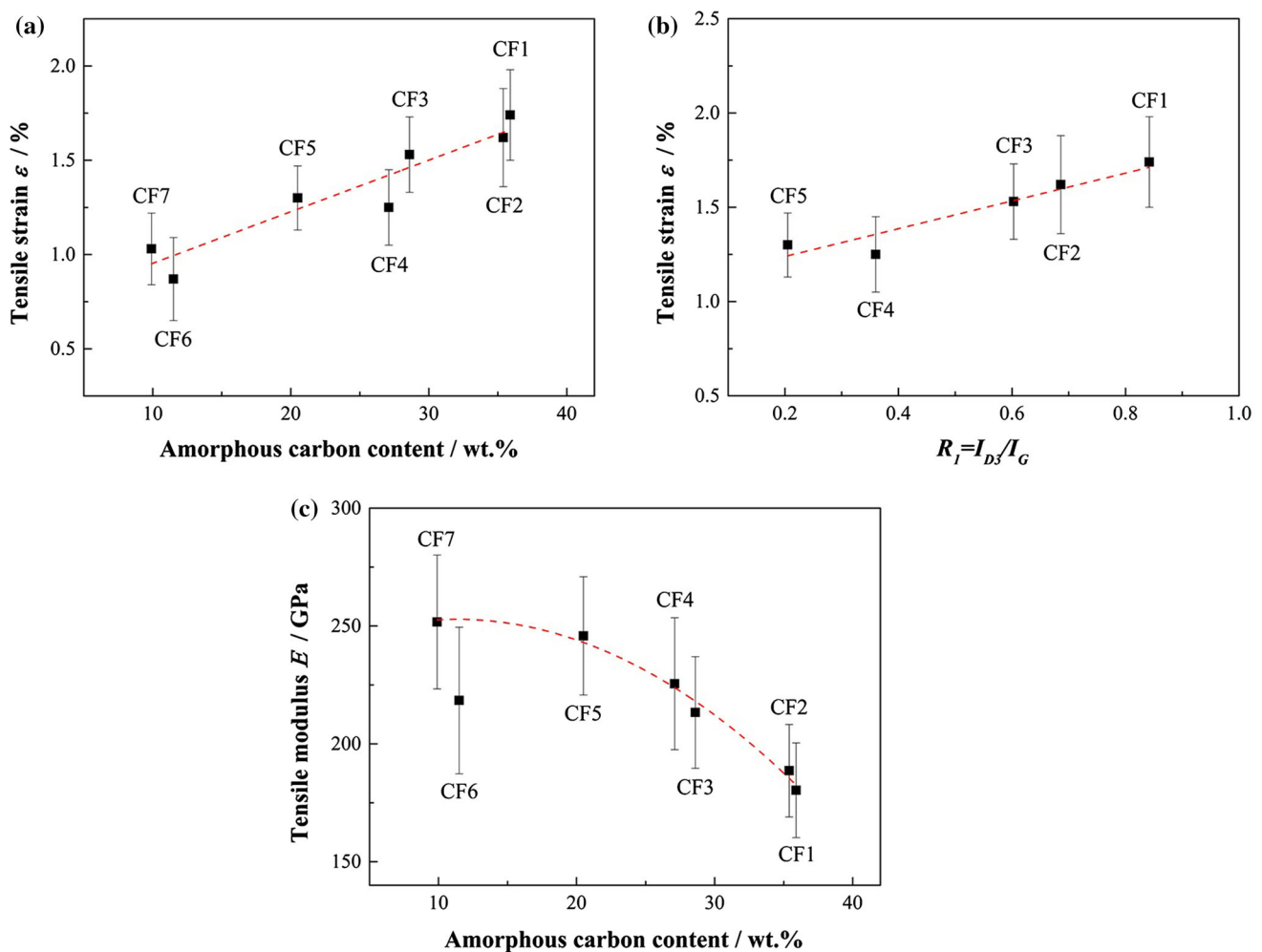
Figure 9 Relationships between the tensile strain and **a** amorphous carbon content, **b** disorder parameter R_1; **c** relationship between the tensile modulus and amorphous carbon content.

based carbon fibers. With the decrease in the amorphous carbon content, the tensile strains of the carbon fibers decrease from 1.74 ± 0.24 to 0.87 ± 0.22%, while the tensile modulus increases from 180 ± 20 to 252 ± 28 GPa. The relationship between the tensile strain and the amorphous carbon content is shown in Fig. 9a. The tensile strains of the carbon fibers are proportional to the amorphous carbon contents,

suggesting that the tensile strain is mainly determined by the amorphous carbon content. According to the fracture surfaces, the crack initiation and propagation mainly occurs in the skin region, and thus the disorder parameter (R_1) provided by quantitative analysis of Raman spectra can also be used to evaluate the tensile strains of the carbon fibers (see Fig. 9b). Unlike the linear relationship between the tensile strain and the amorphous carbon content, a best-fit quadratic curve of the tensile modulus against the amorphous carbon content is shown in Fig. 9c. Because the amorphous carbon modulus is smaller than that of the graphite crystallites [20], the amorphous carbon content is a critical factor influencing the tensile modulus. After graphitization, the theoretical tensile modulus of carbon fiber is increased significantly due to the improvement in the orientation and integrity of graphite crystallites, but the appearance of the structural defects has a negative impact on the tensile modulus of the carbon fibers.

To explain the effect of the microstructure evolution of amorphous carbon on the tensile behavior, the tensile behavior that contained the deformation of the graphite crystallites and amorphous carbon is shown in Fig. 10. Assuming that the stress distribution in the fiber was uniform, it can be inferred that the strain distribution in the carbon fibers is not uniform and the tensile strain in the skin region is small. In the case of the as-received carbon fiber, since the amorphous carbon content was the highest, it had the largest tensile strains both in the skin and in the core regions. When the carbon fibers were heat-treated at the carbonization temperatures, the tensile strains in the skin region are lower due to their less amorphous carbon, which demonstrates that the amorphous-to-crystallite transition in the skin region causes the
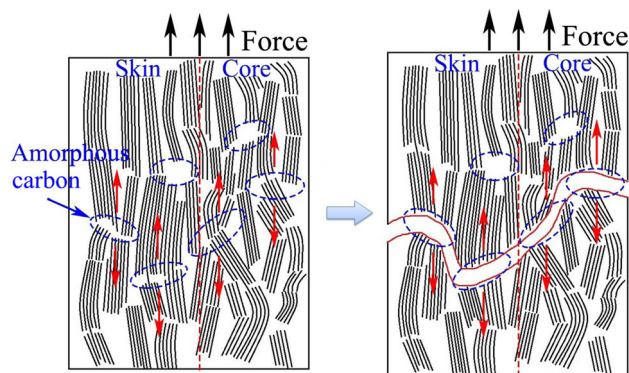
decrease in the tensile strains. However, the increase in the graphite plane improves the cross-linking among graphite crystallites, thereby increasing the tensile strength of the specimen CF3. When the amorphous carbon transforms into perfect graphite crystallites at the graphitization temperatures, although the tensile modulus is increased, the cracks propagate along the structural defects easily, resulting in a significant decrease in the tensile strain and tensile strength.

Conclusions

1. As the heat treatment temperature increases, a large amount of impurity elements are removed and a turbstratic structure of graphite crystallites has become an ordered structure, leading to the increase in the densities of the carbon fibers. The increase in the graphite crystallites has a close relationship with the distribution and microstructure evolution of amorphous carbon; the increase in the graphite crystallite thickness is attributed to the transformation of amorphous carbon (AC1) into graphite planes, while the increase in the graphite crystallite length is resulted from the transformation of amorphous carbon (AC2) and the coalescence between two adjacent graphite crystallites.

2. The Raman spectra analysis by curve fitting provides a quantitative evidence of the microstructure evolution in the skin region of PAN-based carbon fibers. The decrease in the disorder parameter R_1 is attributed to the transformation of sp^2-bonded amorphous carbon into ordered graphite crystallites. Due to the improvement in the integrity and ordering of graphite crystallites, the integrated intensity ratio R_2 decreases significantly at graphitization temperature.

3. The specimen CF3 has the maximum tensile strength because of the improvement in the cross-linking among graphite crystallites. The structural defects and residual stresses generated during the amorphous-to-crystallite transition are responsible for the strength degradation of the carbon fibers. As the amorphous carbon content decreases, the tensile strains of the carbon fibers decrease, while the tensile modulus increases. The amorphous-to-crystallite transition in the

Figure 10 Tensile behavior of PAN-based carbon fibers.

skin region determined the tensile behavior of PAN-based carbon fibers.

Compliance with ethical standards

Conflict of interest The authors declare that they have no conflicts of interest.

References

[1] Okuda H, Young RJ, Tanaka F, Watanabe J, Okabe T (2016) Tensile failure phenomena in carbon fibres. Carbon 107:474–481

[2] Naito K, Yang JM, Tanaka Y, Kagawa Y (2012) The effect of gauge length on tensile strength and Weibull modulus of polyacrylonitrile (PAN)- and pitch-based carbon fibers. J Mater Sci 47:632–642. https://doi.org/10.1007/s10853-011-5832-x

[3] Wu S, Liu YQ, Ge YC, Ran LP, Peng K, Yi MZ (2016) Surface structures of PAN-based carbon fibers and their influences on the interface formation and mechanical properties of carbon-carbon composites. Compos A 90:480–488

[4] Park SJ, Cho MS (2000) Thermal stability of carbon-MoSi$_2$-carbon composites by thermogravimetric analysis. J Mater Sci 35(14):3525–3527. https://doi.org/10.1023/A:1004849110311

[5] Ly HQ, Taylor R, Day RJ (2001) Carbon fibre-reinforced CMCs by PCS infiltration. J Mater Sci 36(16):4027–4035. https://doi.org/10.1023/A:1017990709819

[6] Penev ES, Artyukhov VI, Yakobson BI (2015) Basic structural units in carbon fibers: Atomistic models and tensile behavior. Carbon 85:72–78

[7] Li DH, Lu CX, Wang LN, Du SJ, Yang Y (2017) A reconsideration of the relationship between structural features and mechanical properties of carbon fibers. Mater Sci Eng A 685:65–70

[8] Li DF, Wang HJ, Wang XK (2007) Effect of microstructure on the modulus of PAN-based carbon fibers during high temperature treatment and hot stretching graphitization. J Mater Sci 42(12):4642–4649. https://doi.org/10.1007/s10853-006-0519-4

[9] Wu S, Yi MZ, Ge YC, Ran LP, Peng K (2017) Effect of carbon fiber reinforcement on the tribological performance and behavior of aircraft carbon brake discs. Carbon 117:279–292

[10] Chen TF, Gong WP, Liu GS (2006) Effects of fiber-types on braking behavior of carbon–carbon composites. Mater Sci Eng A 441(1):73–78

[11] Swolfs Y, Shi J, Meerten Y, Hine P, Ward I, Verpoest I, Gorbatikh L (2015) The importance of bonding in intralayer carbon fibre/self-reinforced polypropylene hybrid composites. Compos A 76:299–308

[12] Trinquecoste M, Carlier JL, Derré A, Delhaès P, Chadeyron P (1996) High temperature thermal and mechanical properties of high tensile carbon single filaments. Carbon 34(7):923–929

[13] Saudér C, Lamon J, Paillér R (2004) The tensile behavior of carbon fibers at high temperatures up to 2400 °C. Carbon 42(4):715–725

[14] Zhou GH, Byun JH, Lee SB et al (2014) Nano structural analysis on stiffening phenomena of PAN-based carbon fibers during tensile deformation. Carbon 76:232–239

[15] Guigon M, Oberlin A, Desarmot G (1984) Microtexture and structure of some high tensile strength, PAN-base carbon fibres. Fibre Sci Technol 20(3):177–198

[16] Liu FJ, Wang HJ, Xue LB, Fan LD, Zhu ZP (2008) Effect of microstructure on the mechanical properties of PAN-based carbon fibers during high-temperature graphitization. J Mater Sci 43(12):4316–4322. https://doi.org/10.1007/s10853-008-2633-y

[17] Nunna S, Naebe M, Hameed N, Fox BL, Creighton C (2017) Evolution of radial heterogeneity in polyacrylonitrile fibres during thermal stabilization: an overview. Polym Degrad Stab 136:20–30

[18] Huang Y, Young RJ (1995) Effect of fibre microstructure upon the modulus of PAN- and pitch-based carbon fibres. Carbon 33(2):97–107

[19] Zhou GH, Liu YQ, He L, Guo QG, Ye HQ (2011) Microstructure difference between core and skin of T700 carbon fibers in heat-treated carbon/carbon composites. Carbon 49:2883–2892

[20] Johnson DJ (1987) Structure-property relationships in carbon fibres. J Phys D Appl Phys 20:286–291

[21] Rennhofer H, Loidl D, Puchegger S, Peterlik H (2010) Structural development of PAN-based carbon fibers studied by in situ X-ray scattering at high temperatures under load. Carbon 48:964–971

[22] Fischer L, Ruland W (1980) The influence of graphitization on the mechanical properties of carbon fibers. Colloid Polym Sci 258:917–922

[23] Northolt MG, Veldhuizen LH, Jansen H (1991) Tensile deformation of carbon fibers and the relationship with the

modulus for shear between the basal planes. Carbon 29:1267–1279

[24] Shioya M, Hayakawa E, Takaku A (1996) Non-hookean stress-strain response and changes in crystallite orientation of carbon fibres. J Mater Sci 31:4521–4532. https://doi.org/10.1007/BF00366347

[25] Hong SK, Shioya M, Takaku A (1999) Kinetic studies on hot-stretching of polyacrylonitrile-based carbon fibres by using internal resistance heating. Part II: changes in structure and mechanical properties. J Mater Sci 34(14):3307–3314. https://doi.org/10.1023/A:1004664611696

[26] Qin XY, Lu YG, Xiao H, Wen Y, Tu T (2012) A comparison of the effect of graphitization on microstructures and properties of polyacrylonitrile and mesophase pitch-based carbon fibers. Carbon 50(12):4459–4469

[27] Tanaka F, Okabe T, Okuda H, Ise Kinloch IA, Mori T, Young RJ (2013) The effect of nanostructure upon the deformation micromechanics of carbon fibres. Carbon 52:372–378

[28] Zhong YJ, Bian WF, Wang ML (2016) The effect of nanostructure on the tensile modulus of carbon fibers. J Mater Sci 51:3564–3573. https://doi.org/10.1007/s10853-015-9676-7

[29] Tanaka F, Okabe T, Okuda H, Kinloch IA, Young RJ (2014) Factors controlling the strength of carbon fibres in tension. Compos A 57:88–94

[30] Tanaka F, Okabe T, Okuda H, Kinloch IA, Young RJ (2013) The effect of nanostructure upon the compressive strength of carbon fibres. J Mater Sci 48:2104–2110. https://doi.org/10.1007/s10853-012-6984-z

[31] Jawhari T, Roid A, Casado J (1995) Raman spectroscopic characterization of some commercially available carbon black materials. Carbon 33:1561–1565

[32] Sadezky A, Muckenhuber H, Grothe H, Niesner R, Pöschl U (2005) Raman microspectroscopy of soot and related carbonaceous materials: spectral analysis and structural information. Carbon 43:1731–1742

[33] Dippel B, Jander H, Heintzenberg J (1999) NIR FT Raman spectroscopic study of flame soot. Chem Chem Phys 1:4707–4712

[34] Okuda H, Young RJ, Wolverson D, Tanaka F, Yamamoto G, Okabe T (2018) Investigating nanostructures in carbon fibres using Raman spectroscopy. Carbon 130:178–184

[35] Hu HL, Mu XQ (1988) X-ray diffraction technology. Textile Industry Press, Beijing

[36] Naito K, Tanaka Y, Yang JM, Kagawa Y (2008) Tensile properties of ultrahigh strength PAN-based, ultrahigh modulus pitch-based and high ductility pitch-based carbon fibers. Carbon 46:189–195

[37] Kim M, Jang D, Tejima S, Cruz-Silva R, Joh H, Kim HC, Lee S, Endo M (2016) Strengthened PAN-based carbon fibers obtained by slow heating rate carbonization. Sci Rep 6:22988

[38] Rahaman MSA, Ismail AF, Mustafa A (2007) A review of heat treatment on polyacrylonitrile fiber. Polym Degrad Stab 92:1421–1432

[39] Gao AJ, Zhao C, Luo S, Tong YJ, Xu LH (2011) Correlation between graphite crystallite distribution morphology and the mechanical properties of carbon fiber during heat treatment. Mater Lett 65:3444–3446